Refined treatment of angular momentum in the event-by-event fission model FREYA

J. Randrup[1] and R. Vogt[2,3]
[1]*Nuclear Science Division, Lawrence Berkeley National Laboratory, Berkeley, California 94720, USA*
[2]*Physics Division, Lawrence Livermore National Laboratory, Livermore, California 94551, USA*
[3]*Physics Department, University of California, Davis, California 95616, USA*
(Received 17 January 2014; revised manuscript received 13 March 2014; published 3 April 2014)

The treatment of angular momentum in the event-by-event fission model Fission Reaction Event Yield Algorithm (FREYA) has been refined to ensure conservation of angular momentum both at scission and during neutron evaporation. While the effect on previously calculated quantities is relatively minor, as expected, the refined model gives a more consistent description of directional correlations.

DOI: 10.1103/PhysRevC.89.044601 PACS number(s): 24.10.−i, 25.85.Ca, 25.85.Ec

I. INTRODUCTION

In our earlier FREYA studies of neutron observables in fission [1–4] angular momentum effects were ignored because they are generally expected to be unimportant. However, that is not the case for photon observables and we therefore included fragment angular momentum in our recent studies of photon observables [5]. Because we found that the photon multiplicities are sensitive to the angular momentum, we have refined the angular momentum treatment in several respects and reexamined both neutron and photon observables with the resulting extended FREYA model.

The present refinements concern two aspects of angular-momentum conservation, one during the scission process when the rotating fragments are formed and the other during the evaporation process when the recoil from an emitted neutron may change the angular momentum of the nucleus. This latter effect is relevant not only for post-scission evaporation from excited fission fragments but also for pre-scission evaporation from compound nuclei that are sufficiently hot to allow higher-chance fission.

Because we expect that the effects of these refinements are small, at least for the neutron and photon observables addressed previously, we treat the angular momentum by classical means. Although the results are then not expected to be fully accurate, they should nevertheless provide an indication of the importance of the refinements and help us judge whether more elaborate (and, hence, more time consuming) treatments are called for.

Section II describes the refined scission treatment that conserves angular momentum, while evaporation from rotating nuclei is described in Sec. III. The enhanced capabilities of the extended model are illustrated in Sec. IV for both spontaneous and induced fission and we compare the refined results to our previous work [3,5] in order to understand the importance of the more advanced treatment. Our concluding remarks are made in Sec. V.

II. FRAGMENT ANGULAR MOMENTA

Following our previous treatment [5], we assume that the fragments acquire their angular momenta at scission, but the present treatment is more comprehensive. In particular, it conserves angular momentum in each individual fission event.

It is assumed that the shape evolution has led the system into a rigidly rotating dinuclear configuration just prior to scission. Let $\boldsymbol{S}_0$ denote the associated total angular momentum. It is rather small for thermal-neutron induced fission and vanishes entirely for spontaneous fission. For the present purposes, we treat the fragments as spheres, for simplicity, and we denote their moments of inertia by $\mathcal{I}_i$ for $i = L, H$. The moment of inertia of the relative fragment motion is given by $\mathcal{I}_R = \mu R^2$, where $\boldsymbol{R} = \boldsymbol{R}_L - \boldsymbol{R}_H$ is the position of the light fragment relative to the heavy one and $\mu \approx m_N A_L A_H/(A_L + A_H)$ is the reduced mass of the fragments with m_N being the nucleon mass.

It is convenient to introduce a pre-scission coordinate system by choosing the z axis along the dinuclear axis, $\hat{\boldsymbol{z}} = \boldsymbol{R}/R$, and the y axis along the overall angular momentum, $\hat{\boldsymbol{y}} = \boldsymbol{S}_0/S_0$. It then follows that $\hat{\boldsymbol{x}} = \hat{\boldsymbol{y}} \times \hat{\boldsymbol{z}}$.

Upon scission each of the two fragments will inherit its share of $\boldsymbol{S}_0$. The fragment spins will then be $\boldsymbol{S}_i = (\mathcal{I}_i/\mathcal{I})\boldsymbol{S}_0$, where $\mathcal{I} = \mathcal{I}_L + \mathcal{I}_H + \mathcal{I}_R$ is the total moment of inertia. The remainder of $\boldsymbol{S}_0$ will become the angular momentum of the relative fragment motion, $\boldsymbol{L} = \mu \boldsymbol{R} \times \boldsymbol{U} = (\mathcal{I}_R/\mathcal{I})\boldsymbol{S}_0$, where $\boldsymbol{U} = \dot{\boldsymbol{R}}_L - \dot{\boldsymbol{R}}_R$ is the relative fragment velocity.

In addition to the above average fragment spins arising from the overall dinuclear rotation, the two fragments also acquire fluctuating amounts, $\delta\boldsymbol{S}_L$ and $\delta\boldsymbol{S}_H$. Generally, a dinuclear system has six normal modes of rotation [6], namely *tilting* and *twisting*, in which the fragments rotate in the same or in the opposite sense around the dinuclear axis $\boldsymbol{z}$, and *wriggling* and *bending*, in which the fragments rotate in the same or in the opposite sense around an axis perpendicular to the dinuclear axis. (The two latter types of modes are then each doubly degenerate, corresponding to rotations around $\boldsymbol{x}$ and $\boldsymbol{y}$, for example.) As in Ref. [5], we consider only the latter four modes because the agitation of the former two tends to be suppressed due to the constricted neck [6].

The contribution to the rotational energy from these four dinuclear rotational modes is given by

$$\delta E_{\rm rot} = \boldsymbol{s}_+^2/2\mathcal{I}_+ + \boldsymbol{s}_-^2/2\mathcal{I}_-, \tag{1}$$

where the normal modes have the form $\boldsymbol{s}_\pm = (s_\pm^x, s_\pm^y, 0)$, with the plus referring to the wriggling modes (in which the rotations of the two fragments are parallel) and the minus to the bending modes (in which the rotations of the two fragments

are opposite). The associated moments of inertia are

$$\mathcal{I}_+ = (\mathcal{I}_L + \mathcal{I}_H)\mathcal{I}/\mathcal{I}_R, \quad \mathcal{I}_- = \mathcal{I}_L\mathcal{I}_H/(\mathcal{I}_L + \mathcal{I}_H). \tag{2}$$

It is assumed that these normal dinuclear rotational modes are being agitated statistically during the scission process. Thus, in each event, the values of $\boldsymbol{s}_\pm$ are being sampled from distributions of the form

$$P_\pm(\boldsymbol{s}_\pm = (s_\pm^x, s_\pm^y, 0))ds_\pm^x ds_\pm^y \sim \mathrm{e}^{-s_\pm^2/2\mathcal{I}_\pm T_S} ds_\pm^x ds_\pm^y, \tag{3}$$

where the "spin temperature" T_S is regarded as a global but somewhat adjustable parameter.

Other recent Monte Carlo calculations of prompt photon emission from fission fragments [7–9] do not keep track of the fragment spin directions but consider only their magnitudes. Integer values of these, J_i, are sampled independently for each fragment from distributions of the form $P(J_i) \sim (2J_i + 1)\exp(J_i(J_i+1)/2\sigma^2)$ [9] or $P(J_i) \sim (2J_i+1)\exp((J_i + \frac{1}{2})^2/2\sigma^2)$ [7,8] where the spin cut-off parameter σ is either [7] specified, $\sqrt{2}\sigma = 6\hbar$ for light fragments and $\sqrt{2}\sigma = 7.2\hbar$ for heavy fragments, or [8,9] taken from the RIPL3.0 data library [10].

The corresponding fluctuating angular momentum components of the individual fragments in our approach are then

$$\delta S_L^k = (\mathcal{I}_L/\mathcal{I}_+)s_+^k + s_-^k, \quad \delta S_H^k = (\mathcal{I}_H/\mathcal{I}_+)s_+^k - s_-^k, \tag{4}$$

for $k = x, y$, whereas $\delta S_i^z = 0$. Consequently, the total angular momenta of the fragments are $\boldsymbol{S}_i' = \boldsymbol{S}_i + \delta\boldsymbol{S}_i$.

The resulting orbital angular momentum is then $\boldsymbol{L}' = \boldsymbol{L} - \delta\boldsymbol{S}_L - \delta\boldsymbol{S}_H$. Because the geometrical configuration has not been affected by the angular momentum fluctuations, the "exit" z axis remains the same, $\boldsymbol{z}' = \boldsymbol{z} = \boldsymbol{R}/R$. However, the exit y axis, being directed along the resulting orbital angular momentum, has changed, $\boldsymbol{y}' \propto \boldsymbol{L}'$, and therefore $\boldsymbol{x}' = \boldsymbol{y}' \times \boldsymbol{z}'$ also differs from $\boldsymbol{x}$.

Because the further relative fragment motion is subject to the dinuclear Coulomb force, the asymptotic fragment motion is not along the direction of the dinuclear scission axis. We estimate the resulting final direction by assuming that the separating fragments follow a Coulomb trajectory with the scission configuration being the closest approach, an approximation that ignores the relatively small initial radial kinetic energy (compared to the nearly 200 MeV gained from the Coulomb push). The resulting effect is very small, of the order of just a few degrees.

III. EVAPORATION FROM ROTATING FRAGMENTS

The FREYA procedure for neutron evaporation has been refined to take account of angular momentum in two regards: The emitting nucleus may generally be rotating and the emitted neutron carries away some angular momentum. The general approach is as follows: First the emission point is selected randomly on the nuclear surface and a neutron is then emitted from the local surface element as usual, but it is subsequently boosted by the local rotational velocity of the emission point and the linear and angular-momentum recoils are taken into account.

Our primary goal is to assess the importance of including these angular-momentum refinements and for this purpose we assume that the evaporating nuclei are spherical. Then the orientation of the shape is unaffected by the nuclear rotation which simplifies the formulas. The treatment below holds in the center of mass system of the evaporating nucleus. The nuclear center of mass reference system xyz is aligned with the adopted external XYZ reference system. Its origin is at the center of mass of the emitting nucleus and it is moving along with its velocity. In this coordinate system, the points (x,y,z) located on the spherical surface of the emitting nucleus are characterized by $x^2 + y^2 + z^2 = R_A^2$, where $R_A = r_0 A^{1/3}$ is the nuclear radius. It is therefore straightforward to sample the emission point $\boldsymbol{r}$,

$$\boldsymbol{r} = (x,y,z) = R_A(\sin\vartheta\cos\varphi, \sin\vartheta\sin\varphi, \cos\vartheta). \tag{5}$$

The nuclear rotation vector is $\boldsymbol{\omega} = \boldsymbol{S}/\mathcal{I}$. The rotational velocity $\boldsymbol{w}$ at the emission point $\boldsymbol{r}$ is then

$$\boldsymbol{w}(\boldsymbol{r}) = (w_x.w_y,w_z) = \boldsymbol{\omega}\times\boldsymbol{r}. \tag{6}$$

In order to sample the local velocity of the emitted neutron, we need to introduce a local reference system abc, where $\boldsymbol{c}$ points outwards along the local surface normal (thus the ab plane is tangential to the surface at the emission point $\boldsymbol{r}$). Because the shape is a sphere the local normal is directed along $\boldsymbol{r}$, so $\boldsymbol{c} = \boldsymbol{r}/r$. Choosing $\boldsymbol{b}$ to lie in the XY plane, we then use

$$\boldsymbol{a} = \boldsymbol{b}\times\boldsymbol{c} = (\cos\vartheta\cos\varphi, \cos\vartheta\sin\varphi, -\sin\vartheta), \tag{7}$$

$$\boldsymbol{b} = \boldsymbol{c}\times\boldsymbol{a} = (-\sin\varphi, \cos\varphi, 0), \tag{8}$$

$$\boldsymbol{c} = \boldsymbol{a}\times\boldsymbol{b} = (\sin\vartheta\cos\varphi, \sin\vartheta\sin\varphi, \cos\vartheta). \tag{9}$$

To sample the emission velocity $\boldsymbol{u}$ in the local comoving abc frame, we first sample the emission energy ϵ as before using $P(\epsilon) \sim \epsilon\exp(-\epsilon/T_{\max})$ and then sample its (outwards) direction (θ_n,ϕ_n) (where the polar angle θ_n is measured relative to the local surface normal $\boldsymbol{c}$) from a distribution biased by the normal component $\cos\theta_n$: $\cos^2\theta_n = \eta$ and $\phi_n = 2\pi\eta'$ (where η and η' are random numbers uniform on $(0,1]$), therefore

$$\boldsymbol{u} = u\sin\theta_n\cos\phi_n\boldsymbol{a} + u\sin\theta_n\sin\phi_n\boldsymbol{b} + u\cos\theta_n\boldsymbol{c}. \tag{10}$$

Because the sampled energy ϵ is the kinetic energy of the relative motion of the emitted neutron and the residual daughter nucleus, we have (nonrelativistically) $\epsilon = \frac{1}{2}\mu u^2$, where μ is the reduced mass, $1/\mu = 1/m_n + 1/M'$.

The local velocity of the emitted neutron is therefore $\boldsymbol{u}_n = \boldsymbol{u}/(1 + m_n/M')$ and its total velocity in the center of mass of the emitting nucleus is $\boldsymbol{v} = \boldsymbol{u}_n + \boldsymbol{w}$, where $\boldsymbol{w}$ is the local boost from the rotation (6). Its momentum is then $\boldsymbol{p} = m_n\boldsymbol{v}$. Momentum conservation dictates that the momentum of the daughter nucleus be $\boldsymbol{P}' = -\boldsymbol{p}$, in the center of mass of the mother nucleus.

Furthermore, by angular momentum conservation, we may obtain the angular momentum of the daughter nucleus, $\boldsymbol{S}' = \boldsymbol{S} - \boldsymbol{\ell}$, where $\boldsymbol{\ell} = \boldsymbol{r}\times\boldsymbol{p}$ is the angular momentum carried away by the emitted neutron. The corresponding rotational energy of the residue is $E'_{\mathrm{rot}} = (S')^2/2\mathcal{I}'$. The energy balance

then determines Q', the statistical excitation energy of the daughter,

$$Q' = Q - S_n - \epsilon + E_{\rm rot} - E'_{\rm rot}, \tag{11}$$

where Q is the statistical excitation of the mother nucleus and $E_{\rm rot} = S^2/2\mathcal{I}$ is its rotational energy and the neutron separation energy is $S_n = M' + m_n - M$.

The Q value for neutron evaporation, Q_n^*, is equal to the maximum possible statistical excitation in the daughter nucleus, $Q'_{\rm max}$. Without angular momentum taken into account, the softest emission has $\epsilon = 0$ and leads to the maximal excitation energy in the daughter. However, when angular momentum is incorporated, even such an ultrasoft emission generally produces both linear and angular recoils due to the rotational motion of the emission point. Only when the emission point $\boldsymbol{r}$ is at one of the poles (i.e., $\boldsymbol{r}$ is along or opposite the angular momentum $\boldsymbol{S}$) is there no rotational motion $\boldsymbol{w}$ and an ultrasoft emission produces no recoil (i.e., the linear and angular momenta of the daughter nucleus then remain the same as those of the mother). Because the daughter nucleus has a smaller moment of inertia, it will have a larger rotational energy. As a consequence, Q_n^* is correspondingly reduced, as was already taken into account in Ref. [5],

$$Q_n^* = M + S^2/2\mathcal{I} + Q - m_n - M' - S^2/2\mathcal{I}'. \tag{12}$$

Furthermore, as before, it is necessary to verify that a given sampled emission energy ϵ does not violate the bound set by energy conservation (i.e., the resulting statistical excitation Q' must be positive). The inclusion of the rotational motion introduces stricter bounds that depend on the location of the emission point $\boldsymbol{r}$. Therefore a given sampling of ϵ must be repeated more frequently, though still relatively rarely.

IV. ILLUSTRATIVE APPLICATIONS

The above angular momentum refinements have been incorporated into FREYA. In this section, we examine possible observable effects on neutron and photon emission from spontaneous fission of ^{252}Cf and neutron-induced fission of ^{239}Pu.

A. Preparation

Previously, the initial compound nucleus was assumed to have no angular momentum. Consequently, it was characterized by its charge number Z_0, mass number A_0, and total excitation E_0^*. The latter was either specified explicitly or obtained from the kinematics of neutron absorption. In the present refinement, the initial compound nucleus may be rotating, having a total angular momentum $\boldsymbol{S}_0$ which is either specified explicitly or is calculated from the neutron-absorption kinematics.

When $\boldsymbol{S}_0$ is specified, it is assumed that the initial compound nucleus is at rest, $\boldsymbol{P}_0 = \boldsymbol{0}$. The magnitude of the angular momentum, S_0, may be specified to be any value between zero and the maximum allowed by the excitation energy, $S_0^{\rm max} = [2\mathcal{I}_0 E_0^*]^{1/2}$, where the nuclear moment of inertia is taken as $\mathcal{I}_0 = c\frac{1}{5}M_0 r_0^2 A_0^{2/3}$ with M_0 being the mass of the compound nucleus. For the reduction factor, we use $c = 0.5$ as previously [5]. (The simplifying assumption that the compound nucleus is spherical could readily be improved, should it be required.) The orientation of $\boldsymbol{S}_0$ may be either specified or sampled randomly. While it should have no effect on the physical observables, having this control is useful for testing purposes.

To prepare the initial compound nucleus via neutron absorption, we proceed as follows. The kinetic energy E_n of the incoming neutron is specified, as before, and its direction of motion is selected randomly; its momentum is then $\boldsymbol{p}_n$ with $E_n = p_n^2/2m_n$. Subsequently, its impact parameter $\boldsymbol{b}$ is selected randomly, subject to the constraints that it must be perpendicular to $\boldsymbol{p}_n$ and its magnitude cannot exceed the nuclear radius $R_0 = r_0 A_0^{1/3}$. It is assumed that the neutron is then fully absorbed (so the possibility of pre-equilibrium emission is ignored for now). Consequently, the total linear momentum of the resulting compound nucleus is $\boldsymbol{P}_0 = \boldsymbol{p}_n$ and its total angular momentum is $\boldsymbol{S}_0 = \boldsymbol{b} \times \boldsymbol{p}_n$. Following Ref. [5], we assume that the associated rotational energy is given by $E_0^{\rm rot} = S_0^2/2\mathcal{I}_0$. The total excitation energy in the compound nucleus now follows from energy conservation, $E_0^* = S_n + (1 - m_n/M_0)E_n$, and the statistical part of the excitation energy (the "heat") is given by $Q_0 = E_0^* - E_0^{\rm rot}$.

After its preparation, the resulting compound nucleus may evaporate one or more neutrons before it fissions. The treatment of pre-fission neutron evaporation in the presence of angular momentum is carried out as described in Sec. III.

B. Spontaneous fission of ^{252}Cf

The most important rotational effects in fission at low energy arise from the angular momenta of the fragments, primarily acquired at scission. To bring these effects out as clearly as possible, we consider here spontaneous fission where there is no rotation prior to scission nor any pre-fission neutrons emitted.

Specifically, for ^{252}Cf(sf), we compare various scenarios that differ with regard to the fluctuations in the angular momenta of the fission fragments. The degree of angular momentum fluctuation is governed by the parameter c_S, defined as the ratio between the employed spin temperature T_S and the scission temperature $T_{\rm sc}$. We consider $c_S = 0.0$, $c_S = 0.1$, and $c_S = 1.0$. The value $c_S = 0$ is equivalent to the absence of spin fluctuations at scission. The other two values are chosen to match the results for the Detector for Advanced Neutron Capture Experiments (DANCE) photon multiplicity [11] ($c_S = 0.1$) and the approximate average total emitted photon energy found in earlier measurements [12,13] ($c_S = 1.0$). In the different scenarios, the FREYA parameters e_0 and x are left fixed to simple values close to those determined earlier [4], while the shift dTKE has been adjusted to ensure that the average neutron multiplicity $\overline{\nu}$ is approximately the same in all scenarios. These parameter values are listed in Table I together with the resulting mean magnitudes of the angular momenta of the initial (i.e., pre-evaporation) light and heavy fission fragments.

In scenario 0 the primary fission fragments are not endowed with any angular momentum fluctuations and, because we are considering spontaneous fission, the average fragment

TABLE I. The three scenarios considered for spontaneous fission of ^{252}Cf which are distinguished by the value of the factor $c_S = T_S/T_{sc}$ that governs the magnitude of the fragment spin fluctuations. The values of the usual FREYA parameters e_0, x and dTKE (in MeV) as shown for each scenario, the latter having been adjusted so the resulting average neutron multiplicity $\overline{\nu}$ is approximately the same for all scenarios. Also shown are the resulting mean magnitudes of the angular momenta of the initial light and heavy fission fragments, $\overline{S}_L$ and $\overline{S}_H$.

^{252}Cf(sf)	e_0	x	dTKE	$\overline{\nu}$	$\overline{S}_L$ ($\hbar$)	$\overline{S}_H$ ($\hbar$)
0: $c_S = 0.0$	10	1.3	2.6	3.76	0.02	0.02
1: $c_S = 0.1$	10	1.3	2.4	3.76	1.82	2.25
2: $c_S = 1.0$	10	1.3	0.5	3.75	6.16	7.63

angular momenta also vanish initially. In the course of the evaporation chain, the recoil from each evaporated neutron adds a fluctuating amount of angular momentum to the fragments. This effect is relatively modest: On average, an evaporated neutron carries off about one unit of $\hbar$, the average amount being $\overline{\ell} = 1.09$, 1.10, 1.12 for scenarios 0, 1, and 2, respectively. The slight increase in $\overline{\ell}$ is due to the increase in the typical nuclear rotational frequency with c_S.

1. Neutron observables

Because dTKE is adjusted to ensure that the overall mean neutron multiplicity is the same in the different scenarios, the various other neutron observables are not very sensitive to the degree of fragment rotation. For example, the dependence of the neutron multiplicity on the fragment mass, $\overline{\nu}(A)$, comes out practically the same in all scenarios, as does the total neutron multiplicity distribution, $P(\nu)$.

The effect on the angular correlation between the evaporated neutrons is relatively small, as illustrated quantitatively in Fig. 1. There is a tendency for the correlation pattern to be slightly eroded by the presence of larger angular momenta (scenario 2). The scenario without fluctuations, $c_S = 0$, yields a correlation function that is indistinguishable from that of scenario 1. However, because FREYA provides complete events, it is possible to extract quantities that exhibit larger effects of the degree of fragment rotation, although those "observables" may not be so readily measured experimentally.

For example, one would expect that the angular distribution of neutrons evaporated from a rotating nucleus will acquire an oblate shape, due to the rotational boost that enhances emission in the plane perpendicular to the angular momentum $\boldsymbol{S}$ of the emitting nucleus. Generally, the angular distribution, being symmetric around the direction of $\boldsymbol{S}$, can be analyzed by means of a Legendre expansion. A quantitative measure of the centrifugal effect flattening the neutron angular distribution is then provided by the second Legendre moment,

$$\langle P_2(\cos\theta)\rangle = \left\langle P_2\left(\frac{\boldsymbol{p}\cdot\boldsymbol{S}}{|\boldsymbol{p}||\boldsymbol{S}|}\right)\right\rangle, \tag{13}$$

where $P_2(\cos\theta)$ is the Legendre polynomial of second order. This moment vanishes for isotropic emission patterns; it is positive for prolate distributions (which favor polar emissions), and it is negative for oblate distributions (which favor equatorial emissions). We find $\langle P_2\rangle$ to be -0.002 for scenario 1 and -0.012 for scenario 2, with the corresponding in-plane to out-of-plane ratios of 1.01 and 1.08.

A more detailed impression of this centrifugal effect can be gained from Fig. 2, which shows the various angular distributions of the evaporated neutrons relative to the spin direction of the emitting nucleus, $dv/d\cos\theta_n$, with $\boldsymbol{p}\cdot\boldsymbol{S} = |\boldsymbol{p}||\boldsymbol{S}|\cos\theta_n$. It is seen that although the bias towards equatorial emission increases steadily with c_S the flattening never exceeds a rather modest level. It is perhaps surprising that there is an effect even for scenario 0 in which the fragments are formed without any rotation. This is due to sequential neutron emission: After the first neutron emission a fragment will generally rotate somewhat as a result of the recoil, so subsequent neutron emissions generally occur from nuclei

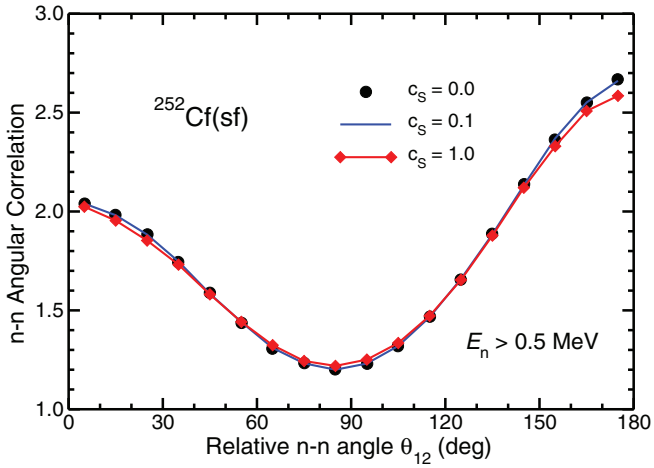

FIG. 1. (Color online) The angular correlation between evaporated neutrons with kinetic energies greater than 0.5 MeV, as obtained from the three scenarios for ^{252}Cf(sf).

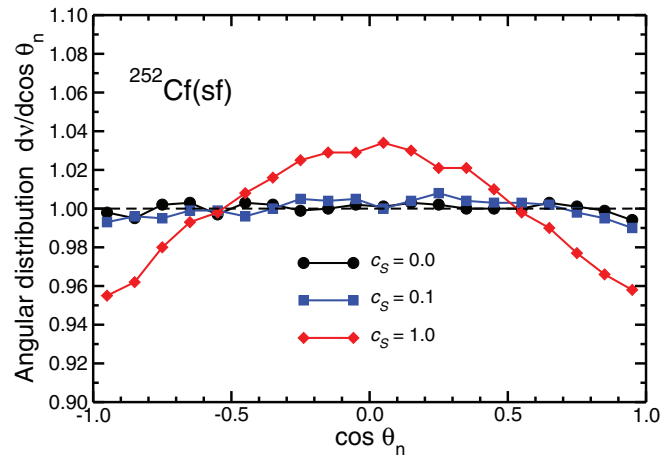

FIG. 2. (Color online) The angular distribution of evaporated neutrons relative to the direction of the angular momentum of the emitting nucleus, as obtained for ^{252}Cf(sf) in the three scenarios.

TABLE II. The average multiplicities of the statistical photons, the subsequent collective photon emission, and the total number of photons for the three scenarios considered. The total multiplicities are compared to recent measured values [11,14].

^{252}Cf(sf)	$\langle N_\gamma^{\rm stat}\rangle$	+	$\langle N_\gamma^{\rm coll}\rangle$	=	$\langle N_\gamma^{\rm total}\rangle$
0: $c_S = 0.0$	6.88		0.70		7.58
1: $c_S = 0.1$	6.89		1.31		8.18
2: $c_S = 1.0$	6.89		4.75		11.64
Ref. [11]	—		—		8.14 ± 0.40
Ref. [14] $LaBr_3$:Ce	—		—		8.30 ± 0.08
Ref. [14] $CeBr_3$	—		—		8.31 ± 0.10

that rotate and they will therefore be subject to the associated centrifugal force.

While the above results are in accordance with general expectations, it is clear that the degree of oblateness remains relatively small even in the presence of large spin fluctuations (scenario 2). This helps explain why the neutron-neutron angular correlations are so relatively insensitive to the fragment rotations (see Fig. 1).

It would be interesting to compare the above FREYA results with results obtained with more refined treatments, such as the Hauser-Feshbach model. However, such comparisons are not straightforward to make because the commonly employed implementations of the Hauser-Feshbach model do not keep track of the angular momentum orientations.

2. Photon observables

Photon emission displays a more significant sensitivity to the fragment rotation. For each of the scenarios, Table II shows the average multiplicity of statistical and collective photons, as well as the total photon multiplicity. The latter increases noticeably with c_S. This increase comes nearly exclusively from the increase in collective photons, whereas the statistical photon emission is largely insensitive to the rotation. This feature is reasonable because the statistical photons depend on the amount of heat present in the nucleus, which is essentially determined by the neutron separation energy, whereas the number of collective photons is directly proportional to the magnitude of the nuclear angular momentum at the end of the statistical emission.

Because the enhanced angular-momentum fluctuations lead to more photons, the photon multiplicity distributions noticeably differ for the three scenarios, as is brought out in Fig. 3. As discussed in Ref. [5], the DANCE multiplicity [11] can be reproduced assuming a rather low contribution from collective photon emission, $c_S \approx 0.1$. The more recent measurement by Billnert *et al.* is similar to this result; see Table II. However, earlier measurements of the total emitted photon energy [12,13] suggest higher values than obtained in scenario 1. Instead, the scenario with $c_S = 1.0$ gives an average radiated energy of $\langle E_\gamma\rangle \sim 7$ MeV, which is closer to the older measured values, $\langle E_\gamma\rangle \sim 6.7 \pm 0.4$ MeV [13]. This energy measurement is consistent with the newer results, $\langle E_\gamma\rangle \sim 7.65 \pm 0.55$ MeV [11] and $\langle E_\gamma\rangle \sim 6.65 \pm 0.12$ MeV (with $CeBr_3$) [14]. More work is still needed to understand the differences between these scenarios and the data.

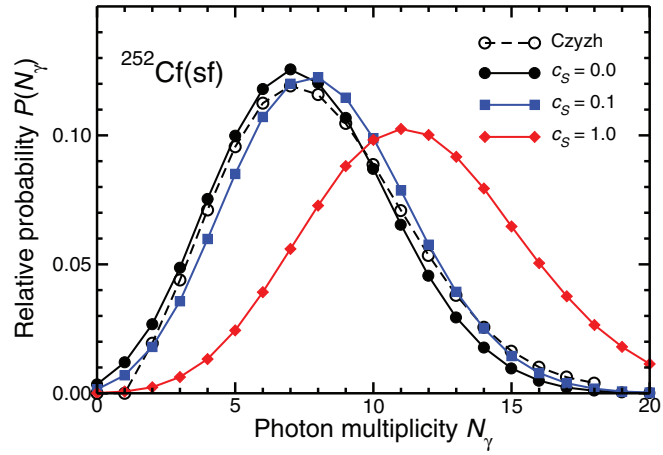

FIG. 3. (Color online) The photon multiplicity distribution obtained for the three scenarios considered compared to the DANCE data [11].

C. Thermal neutron-induced fission of ^{239}Pu

In order to illustrate the angular momentum effects for fission of initially rotating nuclei, we also consider thermal-neutron induced fission, namely ^{239}Pu($n_{\rm th}$,f). The absorption of the incoming neutron endows the resulting compound nucleus, ^{240}Pu*, with a (small) angular momentum $\boldsymbol{S}_0$. Thus the scission configuration is (slowly) rotating and, as a consequence, the nascent fission fragments have a nonvanishing (though small) average angular momentum component directed along $\boldsymbol{S}_0$, in addition to the fluctuating amounts acquired during scission. Subsequently, the fragment angular momenta are modified slightly by each neutron evaporation.

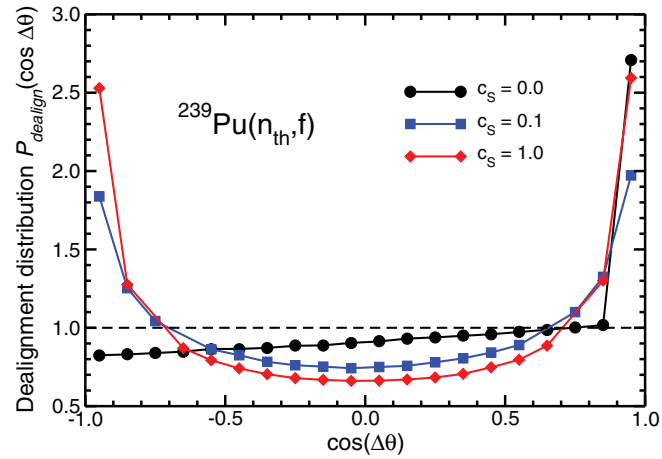

FIG. 4. (Color online) The distribution of the angle between the postevaporation fragment angular momentum and that of the initial compound nucleus, $\Delta\theta$, for $c_S = 0,0.1,1.0$, with dTKE having been adjusted in each scenario to yield $\bar{\nu} = 2.75$.

The refined version of FREYA keeps explicit track of these features in each event and it is thus possible to extract the directional correlation between the resulting postevaporation fragment angular momentum $\boldsymbol{S}_i'$ and the initial compound angular momentum $\boldsymbol{S}_0$. Figure 4 shows the distribution of the associated dealignment angle $\Delta\theta$, determined by $\boldsymbol{S}_i' \cdot \boldsymbol{S}_0 = S_i' S_0 \cos\Delta\theta$, for the three c_S values in the spin-fluctuation scenarios considered for ^{252}Cf(sf).

In the absence of angular momentum fluctuations, $c_S = 0$, the fragment angular momenta are originally oriented along the overall angular momentum $\boldsymbol{S}_0$. Because the angular momenta are only modified slightly by the evaporation recoils, the resulting dealignement is very small. Consequently, the distribution $P_{\rm dealign}(\cos\Delta\theta)$ is strongly peaked at $\cos(\Delta\theta) \approx 1$. As the angular momentum fluctuations are added, this relatively narrow alignment is gradually being eroded and $P_{\rm dealign}(\cos\Delta\theta)$ develops a second peak near $\cos(\Delta\theta) \approx -1$. This feature appears because the fluctuating components arise from the dinuclear rotational modes which conserve overall angular momentum. Furthermore, it is elementary to show that $P_{\rm dealign}(\cos\Delta\theta) \rightsquigarrow 1/\cos(\Delta\theta)$ in the limit where the fluctuations overwhelm the average, corresponding to $P_{\rm dealign}(\cos\Delta\theta)$ approaching a constant.

V. CONCLUDING REMARKS

In this article we described how the treatment of angular momenta in FREYA has been significantly refined to take account of angular momentum conservation, both during scission when the rotating fragments are formed and in the course of the subsequent neutron evaporation chain. The more complete treatment makes it possible to extract observables that are not accessible by other current approaches. With respect to the various distributions calculated previously [3,5], we find only minor differences, as long as dTKE is adjusted to reproduce $\bar{\nu}$.

ACKNOWLEDGMENTS

We wish to acknowledge helpful discussions with P. Fallon, A. Machiavelli, W. E. Ormand, F. S. Stephens, and P. Talou. This work was performed under the auspices of the US Department of Energy under Contracts No. DE-AC52-07NA27344 (R.V.) and No. DE-AC02-05CH11231 (J.R.). The research of R.V. was also supported by the US Department of Energy National Nuclear Security Administration Office of Nonproliferation and Verification Research and Development.

[1] J. Randrup and R. Vogt, Phys. Rev. C **80**, 024601 (2009).
[2] R. Vogt, J. Randrup, J. Pruet, and W. Younes, Phys. Rev. C **80**, 044611 (2009).
[3] R. Vogt and J. Randrup, Phys. Rev. C **84**, 044621 (2011).
[4] R. Vogt, J. Randrup, D. A. Brown, M. A. Descalle, and W. E. Ormand, Phys. Rev. C **85**, 024608 (2012).
[5] R. Vogt and J. Randrup, Phys. Rev. C **87**, 044602 (2013).
[6] T. Døssing and J. Randrup, Nucl. Phys. A **433**, 215 (1985).
[7] O. Litaize and O. Serot, Phys. Rev. C **82**, 054616 (2010).
[8] D. Regnier, O. Litaize, and O. Serot, Phys. Procedia **31**, 59 (2012).
[9] B. Becker, P. Talou, T. Kawano, Y. Danon, and I. Stetcu, Phys. Rev. C **87**, 014617 (2013).
[10] R. Capote *et al.*, Nucl. Data Sheets **110**, 3107 (2009).
[11] A. Chyzh *et al.*, Phys. Rev. C **85**, 021601(R) (2012).
[12] H. Nifenecker, C. Signarbieux, M. Ribrag, J. Poitou, and J. Matuszek, Nucl. Phys. A **189**, 285 (1972).
[13] E. Nardi, A. Gavron, and Z. Fraenkel, Phys. Rev. C **8**, 2293 (1973).
[14] R. Billnert, F.-J. Hambsch, A. Oberstedt, and S. Oberstedt, Phys. Rev. C **87**, 024601 (2013).